

# Flat-band quantum communication induced by disorder

G. M. A. Almeida,<sup>1,\*</sup> R. F. Dutra,<sup>1</sup> A. M. C. Souza,<sup>2</sup> M. L. Lyra,<sup>1</sup> and F. A. B. F. de Moura<sup>1</sup>

<sup>1</sup>*Instituto de Física, Universidade Federal de Alagoas, 57072-900 Maceió, AL, Brazil*

<sup>2</sup>*Departamento de Física, Universidade Federal de Sergipe, 49100-000 São Cristóvão, SE, Brazil*

We show that a qubit transfer protocol can be realized through a flat band hosted by a disordered  $XX$  spin-1/2 diamond chain. In the absence of disorder, the transmission becomes impossible due to the compact localized states forming the flat band. When off-diagonal disorder is considered, the degeneracy of the band is preserved but the associated states are no longer confined to the unit cells. By perturbatively coupling the sender and receiver to the flat band, we derive a general effective Hamiltonian resembling a star network model with two hubs. The effective couplings correspond to wavefunctions associated with the flat-band modes. Specific relationships between these parameters define the quality of the quantum-state transfer which, in turn, are related to the degree of localization in the flat band. Our findings establish a framework for further studies of flat bands in the context of quantum communication.

## I. INTRODUCTION

Progress in quantum information processing have led us to the so-called noisy-intermediate-scale quantum era [1]. This means that the technology for assembling dozens of qubits to perform simple and proof-of-principle tasks is available [2]. Yet, practical issues persist such as faulty quantum gates and limited control over the processing units. A prominent source of errors, besides decoherence, comes from the manufacturing process of quantum devices. For example, the parameters of a qubit network – such as coupling strengths and local transition energies – might deviate from their original design, culminating in disorder. This can consequently lead to Anderson localization of quantum information [3, 4]. Since disorder cannot be fully suppressed, it is important to consider its influence on the quantum dynamics.

Quantum-state transfer (QST) and entanglement distribution are essential tasks to be performed on quantum networks [5]. A quantum communication channel can be set by a collection of spin-1/2 particles acting as qubits and linked via engineered exchange interactions. An arbitrary qubit state prepared at one end of a 1D chain can be transmitted to the other end by the unitary evolution of the Hamiltonian. This idea was introduced by Bose in Ref. [6] and many other schemes have since been proposed [7–24].

A particular class of spin chains for QST relies on a complete engineering of their couplings. This approach results in a linear spectrum that supports end-to-end perfect state transfer in arrays of any size [7, 8]. High-fidelity QST protocols can also be designed with lower engineering costs by tuning the boundaries of a homogeneous spin chain [10, 11, 17]. Other methods involve the application of strong local magnetic fields in order to effectively decouple the sender and receiver spins from the channel [19].

Under the influence of disorder, the overall performance of any QST scheme is expected to be reduced to some degree. [25–36]. Chains featuring modified boundary couplings are more robust against static noise [23, 31]. When the communicating parties are perturbatively coupled to the channel, the conditions for an end-to-end effective interaction become more flexible because most of the channel modes barely interfere. As such, it is possible to tune the end spins in a way that shields the dynamics from the influence of the strongly localized states [37, 38]. Alternatively, one can harness topological protection against disorder [22, 36].

In this paper, we go beyond the usual 1D schemes to explore a QST protocol on a diamond-like spin-1/2 chain [see Fig. 1] described by the  $XX$  model. Disordered quasi-1D materials, such as nanowires, have been shown to display peculiar strongly correlated phenomena [39–41]. Many quasi-1D networks are known to support flat bands [42–44]. These are dispersionless Bloch bands hosting macroscopic degeneracy, diverging density of states, zero-group velocity, and infinite effective mass [45]. A rich variety of transport regimes, including exotic Anderson transitions [46, 47], can emerge, specially when the system is under the influence of perturbations that slightly lift the degeneracy [41, 48–53].

Here we consider a pair of communicating spins weakly coupled to a diamond channel that hosts a flat band. In the ordered case, the band hosts a set of compact localized states, each restricted to one unit cell of the diamond lattice [43, 44]. When off-diagonal disorder is present, the flat band is preserved but is formed by a distinct set of eigenstates. These modes can be extended and thus mediate QST between the end cells. Remarkably, we observe that the competition between the (topological) compact localization and Anderson localization benefits the QST. Furthermore, an effective model is derived to explain that property. By solving it analytically, we highlight the key ingredients responsible for achieving better fidelities. Our findings can be readily extended to other flat band bipartite lattices.

---

\* gmaalmeida@fis.ufal.br

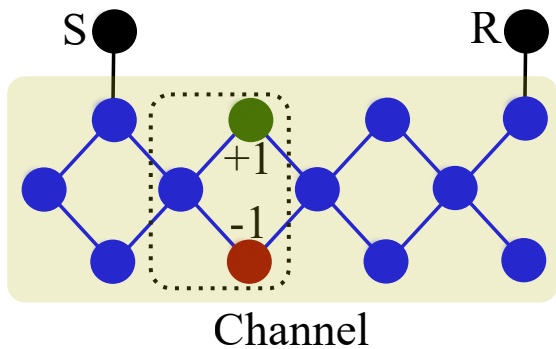


FIG. 1. Sketch of the QST scheme. A quasi-1D diamond lattice functions as the channel. Colored sites with alternating signs inside the unit cell (dashed square) depict the pattern of the compact localized states [43, 44]. These occur in the ordered case and have the form  $|v_0^{(n)}\rangle = \frac{1}{\sqrt{2}}(1, 0, -1)$  for every cell  $n$ . Together, they compose a  $N$ -fold degenerate flat band at  $E = 0$ . Any amount of coupling (off-diagonal) disorder maintains the degeneracy given the bipartite nature of the diamond lattice. On the other hand, the spatial configuration of the flat-band modes will be modified due to their coupling with the dispersive modes. As a consequence, quantum-state transmission between spins  $S$  and  $R$  can be achieved.

## II. MODEL AND FLAT-BAND STRUCTURE

We consider a quantum channel that consists of  $3N$  spin-1/2 particles arranged in a diamond-like configuration with open boundary conditions as shown in Fig. 1. They interact through a  $XX$  Hamiltonian of the form ( $\hbar = 1$ )

$$H_{\text{ch}} = \frac{1}{2} \sum_{\langle i,j \rangle} J_{ij} (\hat{\sigma}_i^x \hat{\sigma}_j^x + \hat{\sigma}_i^y \hat{\sigma}_j^y), \quad (1)$$

where  $\hat{\sigma}_i^{x,y}$  are the usual Pauli operators for spin  $i$  and  $J_{ij}$  is the nearest-neighbour interaction strength between spins  $i$  and  $j$ . Herein, it is more convenient to visualize the channel as being composed of  $N$  coupled vertical trimer cells. In the single-excitation sector, the Hamiltonian reads

$$H_{\text{ch}} = \sum_{n=1}^N (J_{1,n} |a_n\rangle \langle b_n| + J_{2,n} |b_n\rangle \langle c_n|) + \sum_{n=1}^{N-1} (J'_{1,n} |a_n\rangle \langle b_{n+1}| + J'_{2,n} |c_n\rangle \langle b_{n+1}|) + h.c., \quad (2)$$

where  $|\ell_n\rangle$  denotes a single spin flipped in the  $n$ -th cell at leg  $\ell \in \{a, b, c\}$ .

Let us now see how the flat band emerges. Each cell contributes with the local eigenstates  $|v_0^{(n)}\rangle = \frac{1}{\lambda_n} (J_{2,n}, 0, -J_{1,n})$  and  $|v_{\pm 1}^{(n)}\rangle = \frac{1}{\lambda_n \sqrt{2}} (J_{1,n}, \pm \lambda_n, J_{2,n})$ , with corresponding eigenvalues 0 and  $\pm \lambda_n$ , where  $\lambda_n =$

$\sqrt{J_{1,n}^2 + J_{2,n}^2}$ . Within this basis set, transitions between different cells are given by:

$$\langle v_{\nu}^{(n+1)} | H_{\text{ch}} | v_{\pm 1}^{(n)} \rangle = \frac{\nu}{2\lambda_n} (J_{1,n} J'_{1,n} + J_{2,n} J'_{2,n}), \quad (3)$$

$$\langle v_{\nu}^{(n+1)} | H_{\text{ch}} | v_0^{(n)} \rangle = \frac{\nu}{\sqrt{2}\lambda_n} (J_{2,n} J'_{1,n} - J_{1,n} J'_{2,n}), \quad (4)$$

$$\langle v_0^{(n+1)} | H_{\text{ch}} | v_0^{(n)} \rangle = 0, \quad (5)$$

where  $\nu = \pm 1$ .

In the ordered case ( $J_{i,n} = J'_{i,n} = J$ ) a quick look at the expressions above tells us that  $|v_0^{(n)}\rangle$  are eigenstates of  $H_{\text{ch}}$  with the same energy  $E = 0$ . Indeed, they form a complete orthogonal basis at the center of the band. Given each  $|v_0^{(n)}\rangle$  is spatially confined to the  $n$ -th unit cell, they are classified as compact localized states [43, 44]. Therefore, a diamond channel with  $N$  cells hosts a  $N$ -fold degenerate flat band at  $E = 0$ .

The ordered flat band cannot mediate a resonant QST [11] between two external spins weakly coupled to the outermost cells (see Fig. 1). The compact localized states  $|v_0^{(n)}\rangle$  forbid excitation transport between any pair of cells. This scenario changes, however, when  $|v_0^{(n)}\rangle$  are no longer eigenstates of  $H_{\text{ch}}$ . Any disorder in the channel will promote transitions between those and the dispersive modes  $|v_{\nu}^{(n)}\rangle$  [Eq. (4)]. In this work, instead of devising an engineering scheme for  $H_{\text{ch}}$  we will see how random fluctuations in the spin-spin couplings can assist a QST protocol.

Flat-band diamond lattices have been studied in the presence of diagonal as well of off-diagonal disorder [41, 50, 54]. In the weak disorder regime, a general result is that the mixing between flat-band states and the others leads to a scaling of the localization length of the form  $\xi \sim W^{-\gamma}$  at the flat band, with  $W$  being the disorder width and the exponent  $\gamma$  depending on the flat band class [50, 54].

One property that deserves particular attention here is the bipartite nature of the diamond lattice. This means that we can group the  $N$  states  $\{|b_n\rangle\}$  into one sublattice and the remaining  $2N$  states  $\{|a_n\rangle, |c_n\rangle\}$  into another. A known theorem [55, 56] states that bipartite lattices featuring only off-diagonal disorder sustains at least  $M$  linearly independent states at  $E = 0$ , where  $M$  is the difference between the number of sites of both sublattices. In addition, these  $M$  states have no amplitude on the minority sublattice. For the diamond lattice,  $M = N$ .

The flat band is thereby preserved if we set  $J_{i,n} \rightarrow J_{i,n}(1 + \delta_{i,n})$  and  $J'_{i,n} \rightarrow J'_{i,n}(1 + \delta'_{i,n})$ , where  $\delta_{i,n}, \delta'_{i,n}$  are uncorrelated random numbers uniformly distributed in  $[-W/2, W/2]$ . However, note that while the  $N$ -fold degeneracy is maintained at  $E = 0$ , its corresponding modes are no longer  $|v_0^{(n)}\rangle$ . Instead, we get another set of flat-band eigenstates  $|E_{FB,k}\rangle$  which involves linear combinations of  $|v_0^{(n)}\rangle$  and  $|v_{\nu}^{(n)}\rangle$  but still have no amplitude on  $|b_n\rangle$  [55, 56]. Note that as our lattice is finite, there will always be one compact localized state left for the end

cell,  $|v_0^{(N)}\rangle$ . Its contribution is negligible for our purposes. In the following section we show how the disordered flat band can mediate a QST protocol between the outermost cells.

### III. RESULTS

#### A. Effective Hamiltonian

Let us now add two extra spins to the diamond channel, one at each end, to play the role of sender ( $S$ ) and receiver ( $R$ ). As shown in Fig. 1, they are coupled to the sites  $|a_1\rangle$  and  $|a_N\rangle$ , respectively. The full Hamiltonian of the system is now given by  $H_{\text{ch}} + H_I$ , with the interaction Hamiltonian

$$H_I = g(|S\rangle\langle a_1| + |R\rangle\langle a_N| + h.c.). \quad (6)$$

Here we assume that  $g$  is much smaller than the gap between the flat band and the non-zero energy states. The dispersion relation of the delocalized states for an infinite ordered diamond lattice reads  $E(k) = \pm 2J\sqrt{1 + \cos k}$ , with  $k$  being the typical wavenumber [50]. Then, the energy of the next non-zero energy states decreases as  $\sim N^{-1}$  and so  $g \ll JN^{-1}$ . This ensures that only the flat-band modes will contribute to the QST dynamics.

The perturbative coupling set by  $g$  delivers a first-order resonant interaction involving  $|S\rangle$ ,  $|E_{FB,k}\rangle$  ( $k = 1, \dots, N$ ), and  $|R\rangle$ . By generalizing the framework of single-mode resonant QST proposed in [11], we obtain the effective Hamiltonian

$$H_{\text{eff}} = g \sum_{k=1}^N (\mu_{1,k}|S\rangle\langle E_{FB,k}| + \mu_{N,k}|R\rangle\langle E_{FB,k}| + h.c.), \quad (7)$$

where the wavefunctions  $\mu_{n,k} = \langle a_n | E_{FB,k} \rangle$  are now effective couplings. Note that the states  $|c_1\rangle$  and  $|c_N\rangle$  can also host the communicating parties without loss of generality. The states  $|b_n\rangle$  have null amplitudes in the flat band and therefore are not suited for the QST protocol.

In matrix form, the Hamiltonian above reads

$$H_{\text{eff}} = g \begin{pmatrix} 0 & 0 & \mu_{1,1} & \mu_{1,2} & \cdots & \mu_{1,N} \\ 0 & 0 & \mu_{N,1} & \mu_{N,2} & \cdots & \mu_{N,N} \\ \mu_{1,1} & \mu_{N,1} & 0 & 0 & & \vdots \\ \mu_{1,2} & \mu_{N,2} & 0 & 0 & & \vdots \\ \vdots & \vdots & & & \ddots & \\ \mu_{1,N} & \mu_{N,N} & \cdots & & & 0 \end{pmatrix}. \quad (8)$$

The effective QST model can be seen as a disordered star network with two hubs. We remark that the disorder featuring in the parameters  $\mu_{n,k}$  traces back to the fluctuations in  $J_{i,n}$  and  $J'_{i,n}$ , with the constraint that  $\eta_m = \sum_k |\mu_{n,k}|^2 \leq 1$ . The presence of disorder generally lead to  $\eta_1 \neq \eta_N$ . We will see shortly that this population imbalance and the degree of localization of the flat band modes dictate the quality of the QST.

#### B. Quantum-state transfer via flat bands

We now analyze the transfer of an arbitrary qubit state  $|\psi\rangle = \alpha|0_S\rangle + \beta|1_S\rangle$  prepared at site  $S$  (see Fig. 1). The remaining spins are set in the ferromagnetic ground state such that  $|\Psi(t=0)\rangle = |\psi\rangle|0_1 0_2 \cdots 0_{3N} 0_R\rangle$ . To evaluate the QST performance at site  $R$ , we compute the input-averaged (over all  $\alpha$  and  $\beta$ ) transfer fidelity [6]:

$$F(t) = \frac{1}{2} + \frac{|f_R(t)|}{3} + \frac{|f_R(t)|^2}{6}. \quad (9)$$

Hence, it suffices to track the evolution of the transition amplitude  $f_R(t) = \langle R | U(t) | S \rangle$  over time, with  $U(t) = e^{-iHt}$  being the quantum time evolution operator.

We now turn our attention back to the effective two-hub star Hamiltonian [Eq. (8)] to obtain an expression for  $f_R(t)$ . Note that it embodies *another* bipartite network featuring  $N$  nodes in one sublattice (the flat band itself) and two nodes ( $|S\rangle$  and  $|R\rangle$ ) in the other. As such, by symmetry arguments [55, 56], the spectrum is composed of the set of eigenvalues  $\{\pm\epsilon_1, \pm\epsilon_2, \{0\}_{N-2}\}$ . The  $N-2$  states at level  $E=0$  do not have amplitude on the minority sublattice and thus will not contribute to the QST protocol. The remaining four eigenstates can be written as

$$|\epsilon_1^\pm\rangle = \frac{1}{\sqrt{2}}(x_S|S\rangle + x_R|R\rangle) \pm \frac{1}{\sqrt{2}}|\phi_1\rangle, \quad (10)$$

$$|\epsilon_2^\pm\rangle = \frac{1}{\sqrt{2}}(y_S|S\rangle + y_R|R\rangle) \pm \frac{1}{\sqrt{2}}|\phi_2\rangle, \quad (11)$$

where  $|\phi_i\rangle$  are linear combinations of the states  $|E_{FB,k}\rangle$ , satisfying  $\langle \phi_1 | \phi_2 \rangle = 0$ . In each of those eigenstates the probability to find the excitation in either of the sublattices is  $1/2$ . This is another remarkable symmetry property of bipartite networks [57]. As  $\{|\epsilon_1^\pm\rangle, |\epsilon_2^\pm\rangle\}$  must be an orthonormal set, we also have that  $y_S = -x_R^*$  and  $y_R = x_S^*$ , with  $|x_R|^2 + |x_S|^2 = 1$ .

Now, expanding  $U(t) = e^{-iHt}$  we obtain

$$\begin{aligned} f_R(t) &= x_S^* x_R (\cos \epsilon_1 t - \cos \epsilon_2 t) \\ &= -2x_S^* x_R \left[ \sin\left(\frac{\epsilon_1 + \epsilon_2}{2}t\right) \sin\left(\frac{\epsilon_1 - \epsilon_2}{2}t\right) \right]. \end{aligned} \quad (12)$$

The primary QST timescale will be dictated by the slower sine function that depends on the gap  $\delta\epsilon = \epsilon_1 - \epsilon_2$ . The transition amplitude  $|f_R(t)|$  reaches its maximum at times  $\tau = m\pi/\delta\epsilon$ , where  $m = n\delta\epsilon/(\epsilon_1 + \epsilon_2)$ , with  $n$  and  $m$  being odd integers. (Strictly,  $m$  is an integer only if  $\delta\epsilon/(\epsilon_1 + \epsilon_2)$  is rational.) Given the QST time  $\tau \propto g^{-1}$  and recalling that  $g \ll JN^{-1}$ , in order to validate the effective Hamiltonian, then  $\tau$  is typically larger than  $O(N)$ .

The maximum amplitude that  $f_R(t)$  can achieve is related to a correlation parameter  $C_{S,R} = 2|x_S^* x_R| = 4|\langle \epsilon_i^\pm | S \rangle \langle R | \epsilon_i^\pm \rangle|$ , which ranges from 0 to 1. It can thus be used to assess the quality of the QST. Figure 2 depicts the time evolution of the transition amplitude during a QST cycle as obtained by exact diagonalization of

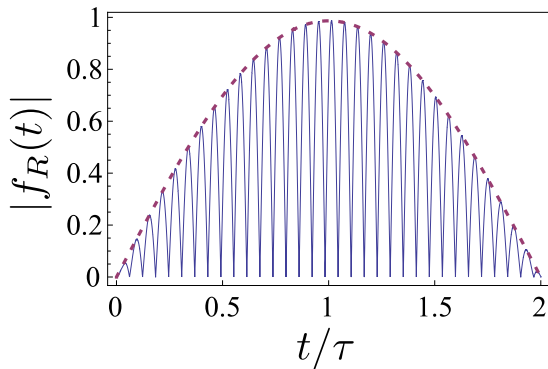


FIG. 2. Time evolution of the transition amplitude  $|f_R(t)|$ . The solid curve is obtained by exact numerical diagonalization of the full Hamiltonian  $H_{\text{ch}} + H_I$  for  $N = 10$  cells,  $g = 0.01J$ , and  $W = 0.2J$ . Only one (typical) disorder realization is shown. The dashed curve represents  $C_{S,R}|\sin(\delta\epsilon t/2)|$ , which is the slow oscillating part of the analytical expression for  $f_R(t)$  in Eq. (12). Both  $C_{S,R}$  and  $\delta\epsilon$  are obtained numerically. Time is expressed in units of the QST time  $\tau = \pi/\delta\epsilon$ .

the full Hamiltonian for a single disorder sample. The wave envelope given by  $C_{S,R}|\sin(\delta\epsilon t/2)|$  is also plotted for comparison.

A perfect QST [within the effective framework of Eq. (8)], with  $F(\tau) = 1$  [Eq. (9)], can only be achieved provided  $C_{S,R} = 1$ , which implies  $|x_S| = |x_R| = 1/\sqrt{2}$ . With regard to the effective couplings  $\mu_{n,k}$ , a particular condition must be fulfilled. To see this, we can solve the eigenvalue equation  $H_{\text{eff}}|\epsilon_i^\pm\rangle = \pm\epsilon_i|\epsilon_i^\pm\rangle$  analytically to obtain:

$$\epsilon_{1,2} = g \left[ \frac{1}{2} \left( A \pm \sqrt{A^2 - 4B} \right) \right]^{1/2}, \quad (13)$$

$$x_S = \left( 1 - \frac{\Lambda^2}{(\tilde{\epsilon}_i^2 - \eta_N)^2 + \Lambda^2} \right)^{1/2}, \quad (14)$$

$$x_R = \frac{\sqrt{2}\Lambda}{\tilde{\epsilon}_i^2 - \eta_N} x_S, \quad (15)$$

where  $A = \eta_1 + \eta_N$ ,  $B = \eta_1\eta_N - \Lambda^2$ ,  $\Lambda = \sum_k(\mu_{1,k}\mu_{N,k})$ , and  $\tilde{\epsilon}_i = \epsilon_i/g$ . Hence, the correlation parameter can be written as  $C_{S,R} = 2/\sqrt{4 + \Delta^2}$ , where  $\Delta = (\eta_1 - \eta_N)/\Lambda$ . We immediately see that  $C_{S,R} = 1$  whenever  $\eta_1 = \eta_N$  (as long as  $\Lambda \neq 0$ ). In such a case, the fluctuations in the parameters  $\mu_{n,k}$  are irrelevant. This is remarkable from the standpoint of the effective Hamiltonian in Eq. (8). It means that in principle one can realize an almost perfect QST despite any level of disorder in  $\mu_{n,k}$  by tuning a *single* parameter.

Here, we cannot manipulate  $\mu_{n,k}$  directly, though. These parameters are attached to the flat-band modes of the physical lattice. Our goal now is to harness the randomness present in the exchange couplings  $J_{i,n}$  and  $J'_{i,n}$ . By doing so, we generally obtain  $\eta_1 \neq \eta_N$  and then  $\Delta \rightarrow 0$  is required to attain  $C_{S,R} \rightarrow 1$ . Note that  $\Delta$  is inversely proportional to the parameter  $|\Lambda| =$

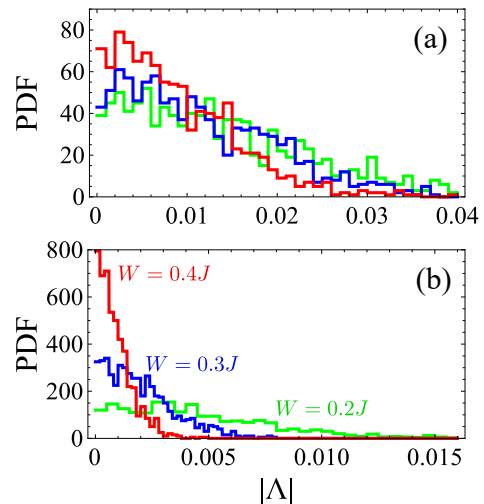


FIG. 3. Probability density functions of the parameter  $|\Lambda| = |\sum_k(\mu_{1,k}\mu_{N,k})|$  evaluated numerically via exact diagonalization of  $H_{\text{ch}}$  considering (a)  $N = 20$  and (b)  $N = 40$  cells for  $10^3$  independent disorder samples. The disorder widths  $W$  considered in both panels are  $0.2J$ ,  $0.3J$ , and  $0.4J$ .

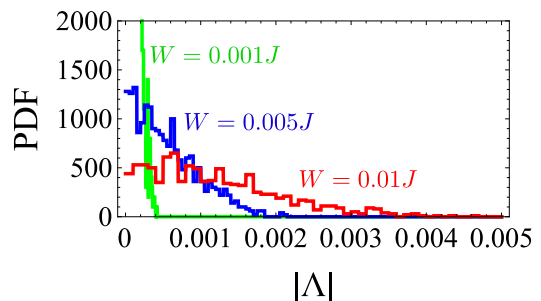


FIG. 4. Probability density functions of  $|\Lambda| = |\sum_k(\mu_{1,k}\mu_{N,k})|$  for the weak disorder regime. Each distribution is obtained for  $10^3$  independent disorder samples considering  $N = 20$ . The disorder widths  $W$  are indicated by each curve.

$|\sum_k(\mu_{1,k}\mu_{N,k})|$ . The latter scans the whole flat band modes via their amplitudes on states  $|a_1\rangle$  and  $|a_N\rangle$  (the ones to which spins  $S$  and  $R$  are coupled). In a disordered system, we expect that the product of two wavefunctions such as  $\mu_{1,k}\mu_{N,k}$  be typically close to zero, especially for spins residing at distant locations.

In Fig. 3 we show probability density functions (PDFs) of  $|\Lambda|$  for  $N = 20, 40$  cells and selected values of the disorder width  $W$ . Indeed, the distributions become more peaked around zero as  $W$  grows. This trend is more severe for larger system sizes [Fig. 3(b)]. Despite the correlation  $C_{S,R}$  is a function of the ratio  $\Delta = (\eta_1 - \eta_N)/\Lambda$ , the factor  $\Lambda$  is the one that counts as far as  $N$  is concerned. This can be observed from the fact that  $\eta_n$  is a local quantity.

Things are different, however, as  $W \rightarrow 0$ . In this regime, we observe the opposite behavior for  $\Lambda$ . The

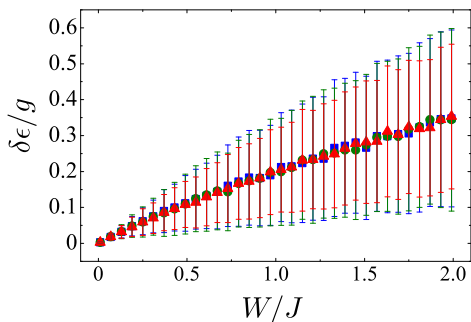


FIG. 5. Energy gap  $\delta\epsilon/g = (\epsilon_1 - \epsilon_2)/g$  versus the disorder width  $W$  for  $N = 10$  (blue squares),  $N = 20$  (green circles), and  $N = 40$  (red triangles). Data are obtained via exact numerical diagonalization of the full Hamiltonian  $H_{\text{ch}} + H_I$ , considering  $g = 0.01J$ , and averaged over  $10^3$  independent realizations of disorder. Error bars are the corresponding mean absolute deviations.

increasing of  $W$  actually benefits the formation of  $C_{S,R}$ . The PDF for very low disorder widths is shown in Fig. 4. Such a reverse trend can be understood as a reminiscent influence of the compact localized states, to which  $\Lambda = 0$ , as we depart from  $W = 0$ . As the disorder increases, the flat-band modes become strongly localized again, but are no longer restricted to each cell. Instead, their localization length scales as  $\xi \sim W^{-\gamma}$  [50, 54]. It is between those two regimes that the QST will occur.

### C. Protocol performance

Now that all the relevant quantities that govern the speed and quality of the QST have been presented, we are ready to test its performance against  $W$ .

Any disorder induces fluctuations in the energy spectrum and affects the transfer time  $\tau \propto \delta\epsilon^{-1}$ . In Fig. 5 we show how the gap  $\delta\epsilon = \epsilon_1 - \epsilon_2$  (in units of  $g$ ) responds to  $W$ . It grows roughly linearly with  $W$ , not being affected by the number of cells  $N$ . Another caveat to the limit  $W \rightarrow 0$  is that a vanishing gap implies in an extremely slow QST, which is not a desirable feature. Therefore, disorder is needed to bypass the compact localized states of the flat band and also to make the QST faster.

Because the fluctuations in the gap increase with  $W$ , we track the QST fidelity over a given time window (instead of a specific time). Let us define  $F_{\text{max}} = \max\{F(t)\}$  as the maximum fidelity achieved for  $t \in [0, t_{\text{max}}]$ , where  $t_{\text{max}} = 20\pi/g$ . Given  $\tau = m\pi/\delta\epsilon$ , we remark that the value of  $t_{\text{max}}$  corresponds to  $m = 1$  and  $\delta\epsilon/g = 0.05$ . In this way, the QST fidelity for disorder widths slightly below  $W \approx 0.2J$  (cf. Fig. 5) may be underestimated. For  $W > 0.2J$ ,  $t_{\text{max}}$  is enough for the first QST cycle to occur [see Eq. (12)].

The results for the QST fidelity are displayed in Fig. 6(a) considering  $N = 10$  and  $N = 20$  cells and fixed  $g = 0.01J$ . Note that this value of  $g$  is compatible with

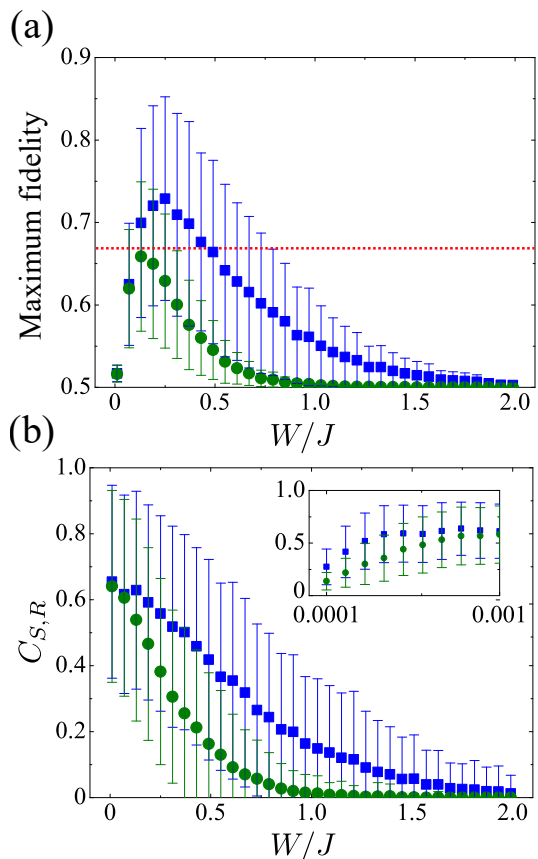


FIG. 6. (a) Maximum fidelity  $F_{\text{max}} = \max\{F(t)\}$ , evaluated for  $t \in [0, 20\pi/g]$ , against  $W$ . Blue squares (green circles) denote the data for  $N = 10$  ( $N = 20$ ), obtained via exact numerical diagonalization of the full Hamiltonian with  $g = 0.01J$ . The dotted horizontal bar indicates the fidelity threshold associated to classical transmission,  $F = 2/3$ . (b) Correlation between spins  $S$  and  $R$ ,  $C_{S,R}$ , also obtained for  $g = 0.01J$ . The inset shows the same measure for smaller values of  $W$ . (The first point lies at  $W = 0.01J$  in the main figures.) Both quantities are averaged over  $10^3$  independent realizations of disorder. Vertical error bars represent the mean absolute deviations.

the system sizes considered. All the elements discussed so far are manifested through the fidelity performances. Indeed, the overall QST quality declines in the larger system size. This has been predicted in the analysis of the parameter  $\Lambda$  (Fig. 3). Yet, it is possible to reach fidelities above the classical threshold of  $2/3$  [6, 58] at intermediate disorder levels. Figure 7 displays histograms of the maximum fidelities for  $N = 10$  and some selected values of  $W$ .

We remark that the poor performances associated to the lower values of  $W$  in Fig. 6(a) is a consequence of the chosen time interval. To confirm this, Fig. 6(b) shows the behavior of correlation  $C_{S,R}$  against  $W$ . As we have seen,  $C_{S,R}$  ultimately determines the quality of the QST. Therefore, in this case higher fidelities *can* be achieved at times  $t > t_{\text{max}}$ . But if we were to consider disorder

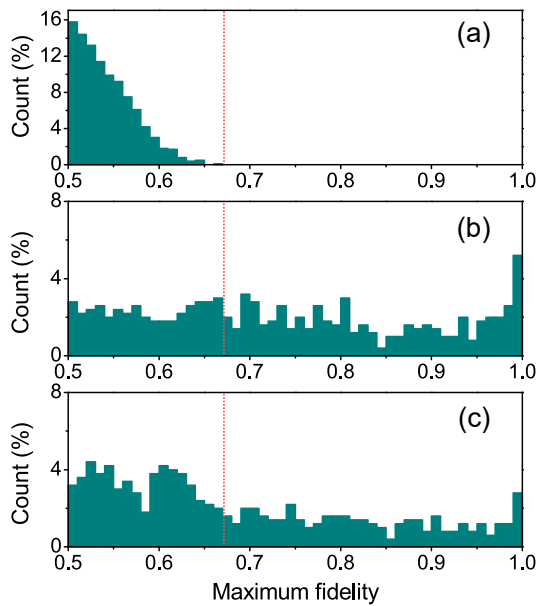


FIG. 7. Histograms of the maximum QST fidelities based on  $10^3$  independent realizations of disorder for  $g = 0.01J$ ,  $N = 10$  cells, (a)  $W = 0.01J$ , (b)  $W = 0.2J$ , and (c)  $W = 0.4J$ . Dotted vertical bars represent the fidelity threshold for classical transmission,  $F = 2/3$ .

levels  $W \ll 0.001J$  [inset of Fig. 6(b)], then the QST would be unfeasible because of the reverse localization trend discussed earlier (see Fig 4). Indeed,  $C_{S,R}$  must vanish as  $W \rightarrow 0$  so as to conform with the development of the compact localized states.

#### IV. CONCLUDING REMARKS

We studied a resonant QST through a flat band hosted by a disordered diamond lattice. In particular, off-

diagonal disorder was considered for preserving the flat band due to the bipartite topology of the lattice. Our findings revealed that the QST protocol yields good fidelities when a certain amount of disorder is present. The underlying phenomenon is a transition of the flat-band modes from compact localization, when  $W = 0$ , to Anderson localization as  $W$  increases [50, 54]. For intermediate levels of disorder, those modes can jointly sustain significant amplitudes on distant cells. While we considered a simple uniform distribution for the disorder, similar results are obtained for uncorrelated Gaussian-distributed disorder (which is a more realistic situation).

We also derived and solved an effective Hamiltonian [Eq. (8)] that applies for a pair of sites perturbatively coupled to any flat-band bipartite lattice. The model resembles a star network with two hubs and disordered couplings associated to the flat-band wavefunctions. By deriving analytical expressions for the relevant eigenstates, we were able to identify the parameters that control the QST. Interestingly, if  $\eta_1 = \eta_N$  then an almost perfect QST can occur for very small  $g$  despite the level of fluctuations associated to the effective couplings  $\mu_{n,k}$ .

The effective model we addressed is a powerful tool to study quantum transport via flat bands. It may be explored on its own as a synthetic network aiming for the remarkable relationship between the couplings. We hope that our results encourage further research on quantum communication in other classes of flat bands [43, 54].

#### V. ACKNOWLEDGMENTS

This work is supported by CNPq, CAPES, FINEP, CNPq-Rede Nanobioestruturas, and FAPEAL.

- 
- [1] J. Preskill, Quantum Computing in the NISQ era and beyond, *Quantum* **2**, 79 (2018).
  - [2] F. Arute *et al*, Quantum supremacy using a programmable superconducting processor, *Nature* **574**, 505 (2019).
  - [3] C. K. Burrell and T. J. Osborne, Bounds on the speed of information propagation in disordered quantum spin chains, *Phys. Rev. Lett.* **99**, 167201 (2007).
  - [4] J. Allcock and N. Linden, Quantum communication beyond the localization length in disordered spin chains, *Phys. Rev. Lett.* **102**, 110501 (2009).
  - [5] H. J. Kimble, The quantum internet, *Nature* **453**, 1023 (2008).
  - [6] S. Bose, Quantum communication through an unmodulated spin chain, *Phys. Rev. Lett.* **91**, 207901 (2003).
  - [7] M. Christandl, N. Datta, A. Ekert, and A. J. Landahl, Perfect state transfer in quantum spin networks, *Phys. Rev. Lett.* **92**, 187902 (2004).
  - [8] M. B. Plenio, J. Hartley, and J. Eisert, Dynamics and manipulation of entanglement in coupled harmonic systems with many degrees of freedom, *New Journal of Physics* **6**, 36 (2004).
  - [9] T. J. Osborne and N. Linden, Propagation of quantum information through a spin system, *Phys. Rev. A* **69**, 052315 (2004).
  - [10] A. Wójcik, T. Łuczak, P. Kurzyński, A. Grudka, T. Gdala, and M. Bednarska, Unmodulated spin chains as universal quantum wires, *Phys. Rev. A* **72**, 034303 (2005).
  - [11] A. Wójcik, T. Łuczak, P. Kurzyński, A. Grudka, T. Gdala, and M. Bednarska, Multiuser quantum communication networks, *Phys. Rev. A* **75**, 022330 (2007).
  - [12] Y. Li, T. Shi, B. Chen, Z. Song, and C.-P. Sun, Quantum-state transmission via a spin ladder as a robust data bus, *Phys. Rev. A* **71**, 022301 (2005).

- [13] M. X. Huo, Y. Li, Z. Song, and C. P. Sun, The Peierls distorted chain as a quantum data bus for quantum state transfer, *Europhysics Letters* **84**, 30004 (2008).
- [14] J. Liu, G.-F. Zhang, and Z.-Y. Chen, Quantum state transfer via a two-qubit Heisenberg xxz spin model, *Physics Letters A* **372**, 2830 (2008).
- [15] G. Gualdi, V. Kostak, I. Marzoli, and P. Tombesi, Perfect state transfer in long-range interacting spin chains, *Phys. Rev. A* **78**, 022325 (2008).
- [16] Z.-M. Wang, M. Byrd, B. Shao, and J. Zou, Quantum communication through anisotropic Heisenberg  $xy$  spin chains, *Physics Letters A* **373**, 636 (2009).
- [17] L. Bianchi, T. J. G. Apollaro, A. Cuccoli, R. Vaia, and P. Verrucchi, Optimal dynamics for quantum-state and entanglement transfer through homogeneous quantum systems, *Phys. Rev. A* **82**, 052321 (2010).
- [18] T. J. G. Apollaro, L. Bianchi, A. Cuccoli, R. Vaia, and P. Verrucchi, 99%-fidelity ballistic quantum-state transfer through long uniform channels, *Phys. Rev. A* **85**, 052319 (2012).
- [19] S. Lorenzo, T. J. G. Apollaro, A. Sindona, and F. Plastina, Quantum-state transfer via resonant tunneling through local-field-induced barriers, *Phys. Rev. A* **87**, 042313 (2013).
- [20] S. Paganelli, S. Lorenzo, T. J. G. Apollaro, F. Plastina, and G. L. Giorgi, Routing quantum information in spin chains, *Phys. Rev. A* **87**, 062309 (2013).
- [21] S. Lorenzo, T. J. G. Apollaro, S. Paganelli, G. M. Palma, and F. Plastina, Transfer of arbitrary two-qubit states via a spin chain, *Phys. Rev. A* **91**, 042321 (2015).
- [22] G. M. A. Almeida, F. Ciccarello, T. J. G. Apollaro, and A. M. C. Souza, Quantum-state transfer in staggered coupled-cavity arrays, *Phys. Rev. A* **93**, 032310 (2016).
- [23] G. M. A. Almeida, Interplay between speed and fidelity in off-resonant quantum-state-transfer protocols, *Phys. Rev. A* **98**, 012334 (2018).
- [24] T. J. G. Apollaro, G. M. A. Almeida, S. Lorenzo, A. Ferraro, and S. Paganelli, Spin chains for two-qubit teleportation, *Phys. Rev. A* **100**, 052308 (2019).
- [25] G. De Chiara, D. Rossini, S. Montangero, and R. Fazio, From perfect to fractal transmission in spin chains, *Phys. Rev. A* **72**, 012323 (2005).
- [26] J. Fitzsimons and J. Twamley, Superballistic diffusion of entanglement in disordered spin chains, *Phys. Rev. A* **72**, 050301 (2005).
- [27] D. Burgarth and S. Bose, Perfect quantum state transfer with randomly coupled quantum chains, *New Journal of Physics* **7**, 135 (2005).
- [28] D. I. Tsomokos, M. J. Hartmann, S. F. Huelga, and M. B. Plenio, Entanglement dynamics in chains of qubits with noise and disorder, *New Journal of Physics* **9**, 79 (2007).
- [29] S. M. Giampaolo and F. Illuminati, Long-distance entanglement in many-body atomic and optical systems, *New Journal of Physics* **12**, 025019 (2010).
- [30] N. Y. Yao, L. Jiang, A. V. Gorshkov, Z.-X. Gong, A. Zhai, L.-M. Duan, and M. D. Lukin, Robust quantum state transfer in random unpolarized spin chains, *Phys. Rev. Lett.* **106**, 040505 (2011).
- [31] A. Zwick, G. A. Álvarez, J. Stolze, and O. Osenda, Spin chains for robust state transfer: Modified boundary couplings versus completely engineered chains, *Phys. Rev. A* **85**, 012318 (2012).
- [32] A. Zwick, G. A. Álvarez, J. Stolze, and O. Osenda, Quantum state transfer in disordered spin chains: how much engineering is reasonable?, *Quant. Inf. Comp.* **15**, 852 (2015).
- [33] M. Bruderer, K. Franke, S. Ragg, W. Belzig, and D. Obreschkow, Exploiting boundary states of imperfect spin chains for high-fidelity state transfer, *Phys. Rev. A* **85**, 022312 (2012).
- [34] S. Ashhab, Quantum state transfer in a disordered one-dimensional lattice, *Phys. Rev. A* **92**, 062305 (2015).
- [35] A. Kay, Quantum error correction for state transfer in noisy spin chains, *Phys. Rev. A* **93**, 042320 (2016).
- [36] M. P. Estarellas, I. D'Amico, and T. P. Spiller, Robust quantum entanglement generation and generation-plus-storage protocols with spin chains, *Phys. Rev. A* **95**, 042335 (2017).
- [37] G. M. A. Almeida, F. A. B. F. de Moura, and M. L. Lyra, High-fidelity state transfer through long-range correlated disordered quantum channels, *Phys. Lett. A* **382**, 1335 (2018).
- [38] G. M. A. Almeida, F. A. B. F. de Moura, and M. L. Lyra, Transmission of quantum states through disordered channels with dimerized defects, *Quant. Inf. Proc.* **18**, 350 (2019).
- [39] A. P. Petrović, D. Ansermet, D. Chernyshov, M. Hoesch, D. Salloum, P. Gougeon, M. Potel, L. Boeri, and C. Panagopoulos, A disorder-enhanced quasi-one-dimensional superconductor, *Nature Communications* **7**, 12262 (2016).
- [40] G. Gligorić, D. Leykam, and A. Maluckov, Influence of different disorder types on aharonov-bohm caging in the diamond chain, *Phys. Rev. A* **101**, 023839 (2020).
- [41] N. Roy, A. Ramachandran, and A. Sharma, Interplay of disorder and interactions in a flat-band supporting diamond chain, *Phys. Rev. Research* **2**, 043395 (2020).
- [42] M. Hyrkäs, V. Apaja, and M. Manninen, Many-particle dynamics of bosons and fermions in quasi-one-dimensional flat-band lattices, *Phys. Rev. A* **87**, 023614 (2013).
- [43] S. Flach, D. Leykam, J. D. Bodyfelt, P. Matthies, and A. S. Desyatnikov, Detangling flat bands into Fano lattices, *EPL* **105**, 30001 (2014).
- [44] W. Maimaiti, A. Andreanov, H. C. Park, O. Gendelman, and S. Flach, Compact localized states and flat-band generators in one dimension, *Phys. Rev. B* **95**, 115135 (2017).
- [45] O. Derzhko, J. Richter, and M. Maksymenko, Strongly correlated flat-band systems: The route from Heisenberg spins to Hubbard electrons, *International Journal of Modern Physics B* **29**, 1530007 (2015).
- [46] M. Goda, S. Nishino, and H. Matsuda, Inverse Anderson transition caused by flatbands, *Phys. Rev. Lett.* **96**, 126401 (2006).
- [47] J. T. Chalker, T. S. Pickles, and P. Shukla, Anderson localization in tight-binding models with flat bands, *Phys. Rev. B* **82**, 104209 (2010).
- [48] A. M. C. Souza and H. J. Herrmann, Flat-band localization in the Anderson-Falicov-Kimball model, *Phys. Rev. B* **79**, 153104 (2009).
- [49] R. A. Vicencio and M. Johansson, Discrete flat-band solitons in the kagome lattice, *Phys. Rev. A* **87**, 061803 (2013).
- [50] D. Leykam, S. Flach, O. Bahat-Treidel, and A. S. Desyatnikov, Flat band states: Disorder and nonlinearity, *Phys. Rev. B* **88**, 224203 (2013).

- [51] A. Ramachandran, A. Andreanov, and S. Flach, Chiral flat bands: Existence, engineering, and stability, *Phys. Rev. B* **96**, 161104 (2017).
- [52] R. Khomeriki and S. Flach, Landau-Zener Bloch oscillations with perturbed flat bands, *Phys. Rev. Lett.* **116**, 245301 (2016).
- [53] G. Bouzerar and D. Mayou, Quantum transport in flat bands and supermetallicity, *Phys. Rev. B* **103**, 075415 (2021).
- [54] D. Leykam, J. D. Bodyfelt, A. S. Desyatnikov, and S. Flach, Localization of weakly disordered flat band states, *The European Physical Journal B* **90**, 1 (2017).
- [55] B. Sutherland, Localization of electronic wave functions due to local topology, *Phys. Rev. B* **34**, 5208 (1986).
- [56] M. Inui, S. A. Trugman, and E. Abrahams, Unusual properties of midband states in systems with off-diagonal disorder, *Phys. Rev. B* **49**, 3190 (1994).
- [57] A. M. C. Souza, R. F. S. Andrade, N. A. M. Araújo, A. Vezzani, and H. J. Herrmann, How the site degree influences quantum probability on inhomogeneous substrates, *Phys. Rev. E* **95**, 042130 (2017).
- [58] M. Horodecki, P. Horodecki, and R. Horodecki, General teleportation channel, singlet fraction, and quasidistillation, *Phys. Rev. A* **60**, 1888 (1999).